

# General-purpose open-source 1D self-consistent Schrödinger-Poisson Solver: Aestimo 1D



H. Hebal<sup>a</sup>, Z. Koziol<sup>b</sup>, S.B. Lisesivdin<sup>c,\*</sup>, R. Steed<sup>d</sup>

<sup>a</sup> Department of Technical Sciences, University of Mohamed Boudiaf, 28000 M'sila, Algeria

<sup>b</sup> National Center for Nuclear Research, Materials Research Laboratory, ul. Andrzeja Sołtana 7, 05-400 Otwock-Świerk, Poland

<sup>c</sup> Department of Physics, Faculty of Science, Gazi University, Teknikokullar, 06500 Ankara, Turkey

<sup>d</sup> European-Mediterranean Seismological Centre, c/o CEA, 91297 Arpajon Cedex, France

## ARTICLE INFO

### Keywords:

Aestimo1D  
Schrödinger-Poisson  
2DEG

## ABSTRACT

We present a general-purpose numerical quantum mechanical solver using Schrödinger-Poisson equations called Aestimo 1D. The solver provides self-consistent solutions to the Schrödinger and Poisson equations for a given semiconductor heterostructure built with materials including elementary, binary, ternary, and quaternary semiconductors and their doped structures. The software can be used to calculate electronic band structures of heterostructures either using a single-band or multi-band k.p envelope function approximation. The software is fully open-source and it is released under the GNU general public license version 3 for full freedom of usage for applications in the fields of nano-electronics, optoelectronics, and solid-state device simulations.

## 1. Introduction

High-demand for technological devices including sensors, LEDs, Lasers, and CMOS has led to pressure for miniaturization [1–4] and this has led many semiconductor devices to be made up of different materials that have dimensions less than 10 nm [5,6] or having layers with quantum-confined carrier gases on the nanometer scale [7,8]. At the nanometer scale, the electronic band structure of quantum confined carrier gases in MOSFETs or HEMTs is highly dependent on parameters like layer thickness, alloy mole fraction, and doping concentration. To produce more effective devices, further investigation of these parameters' effects on device properties is necessary. Generally, the required investigation can be done by computational investigation of a potential distribution among the semiconductor layers and the determination of the electronic energy levels of related low-dimensional carrier populations. With a proper calculation, one can also calculate the possible intersubband transition energies and related intersubband optical properties of these semiconductor devices. These calculations can be done by solving Schrödinger and Poisson equations at least in one-dimension (1D) (which is related to the semiconductor thin film growth direction) self-consistently.

In 2012, Aestimo 1D project is started to develop the first open-source 1D general-purpose quantum mechanical solver, initially for educational purposes, a helpful tool for the coursebook [9]. In 2014, after 10 minor releases, version 1.0 was released. With this release,

Aestimo 1D became a helpful tool for theoretical and experimental research on nano-scale electronic and optoelectronic devices. After 6 years of additional development, the second major version was released in 2020. Version 2.0 includes many new calculation methods, solvers, and improvements to the material database. As a fact, Aestimo 1D is used both in computational-only studies [10] and as a computational tool to verify experimental studies [11–15] for many years. In experimental studies of Erucar *et al.* and Cetinkaya *et al.*, Aestimo 1D is used to calculate electron and heavy-hole/light hole subband energies in Molecular Beam Epitaxy (MBE) grown GaAs<sub>1-x</sub>Bi<sub>x</sub>/AlGaAs heterostructures [11,12]. In these studies, researches modified the standard Varshni equation in a way to include an extra linear temperature-dependent term. These kinds of modifications can be possible because of the open-source nature of the Aestimo 1D. In the experimental studies reported by Bajo *et al.* and Meng *et al.*, the values of allowed intersubband transition energies of the ZnO/Mg<sub>x</sub>Zn<sub>1-x</sub>O multiple QW structures grown by MBE on m-plane ZnO substrates are calculated with Aestimo 1D [13–15]. Successful results of all these studies also show Aestimo 1D can be used in many different applications that having different material systems and can be also modified for case-specific calculations and fit processes.

This paper aims to give basic information about the physical models employed and the usage of the package to show the reliability of those physical models. The methodologies for solving the general self-consistent Schrödinger-Poisson equation and other computational schemes

\* Corresponding author.

E-mail address: [sblisesivdin@gmail.com](mailto:sblisesivdin@gmail.com) (S.B. Lisesivdin).

implemented in Aestimo 1D are presented in Section 2; followed by the structure of the software being described in Section 3. Some examples and comparative results with other solvers are then discussed in Section 4.

## 2. Methods

### 2.1. Computation schemes

At its core, Aestimo 1D is a Schrödinger-Poisson equation solver for stacks of planar layers that have nanometer thickness. The coupled Schrödinger-Poisson equation solution begins by solving a Schrödinger equation (including non-parabolicity effects as necessary) with a special kinetic energy operator and spatial effective mass function to accommodate possible discontinuities at the interface boundaries [9]:

$$-\frac{\hbar^2}{2} \frac{\partial}{\partial z} \frac{1}{m^*(z)} \frac{\partial}{\partial z} \psi(z) + V(z)\psi(z) = E\psi(z) \quad (1)$$

$$\left( \frac{\partial}{\partial z} \varepsilon(z) \frac{\partial}{\partial z} \right) V_P(z) = -\rho(z) \quad (2)$$

where  $V_P(z)$  is the additional potential term arising from charge distribution  $\rho(z)$ , and  $\varepsilon(z)$  is the permittivity of the material.

Once we solve the Schrödinger equation and obtain the band structure wavefunctions, we can calculate the charge distribution, since the absolute value of wavefunctions is related to charge distribution. However, the resulting charge distribution will modify the potential  $V(z)$  for which we solved the original Schrödinger equation. A new value of potential is found by solving the Poisson equation for charge distribution and adding the calculated  $V_P(z)$  potential to previous total potential. Therefore, we ought to solve the Schrödinger equation again, using the new potential, and find again a new charge distribution. We have to repeat these steps over and over again until the results of the latest solution are reasonably close to the results from the previous solution. This well-known method of solving equations is called a self-consistent method and shown in Fig. 1.

In addition to the known self-consistent Schrödinger-Poisson equation solving scheme, Aestimo 1D has many different schemes that can be used in different applications or problems that need different types of calculation: the effects of non-parabolicity of the bands or exchange interaction can be estimated and drift-diffusion calculations can be performed. The different computation schemes can be easily chosen from an input file. Table 1 shows the computation schemes implemented in Aestimo 1D.

### 2.2. Single-band model

Aestimo has a single band model that can be used for modelling structures where the valence band can be neglected entirely. For

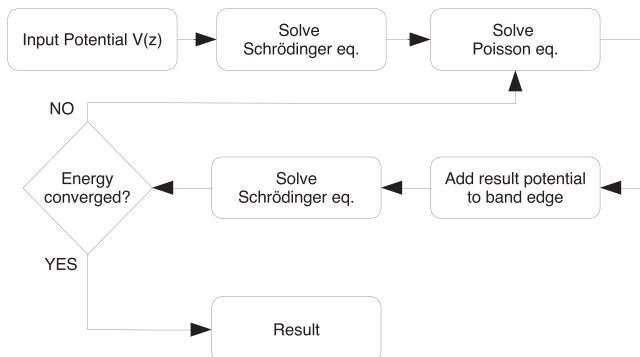


Fig. 1. Schematics of self-consistent Schrödinger-Poisson equation solving scheme.

Table 1

Computational models available in Aestimo 1D.

computation_scheme	Value	Called Model
0		Schrödinger
1		Schrödinger + nonparabolicity
2		Schrödinger-Poisson
3		Schrödinger-Poisson with nonparabolicity
4		Schrödinger-Exchange interaction
5		Schrödinger-Poisson + Exchange interaction
6		Schrödinger-Poisson + Exchange interaction with nonparabolicity
7		Schrödinger-Poisson, Poisson-Drift_Diffusion (Gummel map)
8		Schrödinger-Poisson, Drift_Diffusion (Gummel map)
9		Schrödinger-Poisson, Drift_Diffusion (Gummel & Newton maps)

instance, for modelling the conduction band of GaAs-AlGaAs quantum wells. The model implements the shooting wave procedure for finding the energy levels and wavefunctions for arbitrary heterostructures [9]. In each layer, the conduction band electrons have an effective mass and between each layer, a conduction band offset is defined using a database of material properties. To improve upon this basic model, corrections are made to account for the non-parabolicity of the conduction bands and for the exchange interaction between the electrons.

#### 2.2.1. Non-parabolicity of $E(k)$

The conduction and valence bands of semiconductors are commonly approximated as parabolic around their extrema. This approximation of  $E(k)$  ignores the complexity of the band structure of real materials. It is important to account for this effect in particular in case of narrow quantum wells or higher-lying subbands in wide quantum wells. In Aestimo 1D, conduction band  $E(k)$  approximation is described [16] by the dispersion relation,

$$E(k) = \frac{\hbar^2 k^2}{2m^*} (1 - \gamma k^2) \quad (3)$$

where  $\gamma$  is the non-parabolicity parameter. For multi-band calculations, the 3x3 k.p Hamiltonian accounts for non-parabolic effects of valance band (see Section 2.3).

#### 2.2.2. Exchange interaction

Since electrons are Fermions, two of them cannot occupy the same state when their spins are the same. The same is true for the holes in the valence band. At the same time, electrostatic interactions exist between them. The interaction between these 2 effects can be modeled by adding additional potential, which is called exchange-correlation potential,  $V_{xc}$ . There are approximations used for  $V_{xc}$  that are in practice sufficiently accurate. Exchange interaction plays a more significant role in cases of strong doping (at low temperatures and very low doping levels it may be ignored). An effective field describing the exchange-correlation between the electrons is derived from Kohn-Sham density functional theory [17]. The equation used in Aestimo 1D is,

$$V_{xc} = -A \cdot \frac{n^{1/3}}{\varepsilon} \left( 1 + 0.0545 \cdot r_s \cdot \log \left( 1 + \frac{11.4}{r_s} \right) \right) \quad (4)$$

where  $A = q^2/4\pi \cdot (3/\pi)^{1/3}$ ,  $n$  is the electron density, and  $r_s$  is the average distance between charges.

In equation 4,  $r_s$  is the average distance between charges, and the  $r_s$  is calculated as follows:

$$r_s = \frac{1}{\left( \frac{4\pi m}{3} \right)^{1/3} a_B^*} \quad (5)$$

Here,  $a_B^*$  is the effective Bohr radius which is given as [17]

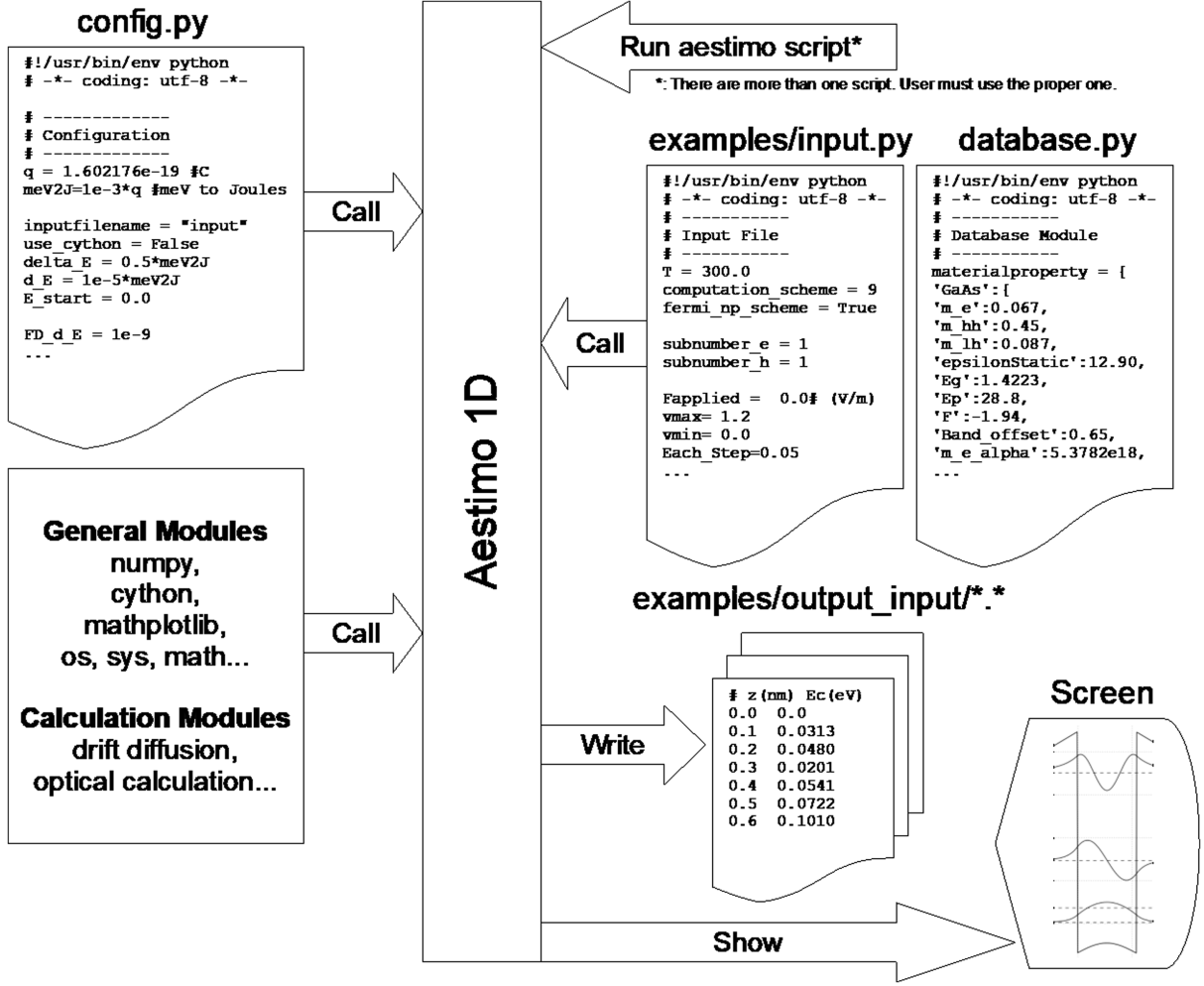


Fig. 2. The working structure of Aestimo 1D.

$$a_B^* = \frac{4\pi\epsilon_s \hbar^2}{m^* q^2} \quad (6)$$

where  $\epsilon_s$  is the static dielectric constant of the related layer.

### 2.3. Multi-band model

The valence band structure is more complex than the conduction band and so a solution using single effective masses for each valence sub-band is not sufficient. For valence band calculations, a 3x3 Hamiltonian is employed for (001)-oriented zinc blende (ZB) and (0001)-oriented wurtzite (WZ) crystals by using k.p theory. Besides, the model considers spontaneous-piezoelectric built-in field dependence and strain effects [18]. Normally, with magnetic field interactions, 6x6 Hamiltonian solutions are necessary. However, because Aestimo 1D does not include magnetic interactions, 3x3 solutions are satisfactory.

The energy bands  $E_c$ ,  $E_v$  and wave functions  $\phi_n^\eta$  and  $\Psi_m$  of conduction and valence bands states respectively, are obtained from a numerical solution of the Schrödinger equations for electrons with the electron wave function is given by

$$|\phi_n^\eta\rangle = e^{ik_x x + ik_y y} \phi_n(z) |S\eta\rangle \quad (5)$$

where  $\eta = \uparrow$  or  $\downarrow$  and  $S$  is a spherically symmetric wavefunction and  $\phi_n$  is the envelope function that satisfies

$$[H_c(k_x, k_y, -i\partial/\partial z) + (v_c(z) + eF_z z)\delta_{vu}] \phi_n(k_x, k_y, z) = E_c(k_x, k_y) \phi_n(k_x, k_y, z) \quad (6)$$

and for holes with the hole wave function is given by

$$|\Psi_m\rangle = \sum_{u=1}^3 [e^{ik_x x + ik_y y} g_m^{(u)}(z) |v\rangle] \quad (7)$$

where  $g_m^{(u)}$  is the envelope function of the  $m^{\text{th}}$  sub-band that satisfies

$$\sum_{\mu=0}^3 [H_{v\mu}(k_x, k_y, -i\partial/\partial z) + (v_h(z) + eF_z z)\delta_{v\mu}] g_m^{(\mu)}(k_x, k_y, z) = E_m(k_x, k_y) g_m^{(\mu)}(k_x, k_y, z) \quad (8)$$

where the potential  $v_h(z)$  ( $v_c(z)$ ) is the potential for the valence (conduction) offset of the QW,  $F_z$  is the internal electric fields with  $e$  as the elementary charge. The built-in electric field is written as [19,20],

$$F_z^w = \frac{(P_{SP}^b + P_{PZ}^b - P_{SP}^w - P_{PZ}^w)}{\epsilon^w + \epsilon^b(L_w/L_b)} \quad (9)$$

$$F_z^b = -\frac{L_w}{L_b} F_z^w$$

where  $P_{SP/PZ}^w/P_{SP/PZ}^b$ ,  $L_w(L_b)$  and  $\epsilon_w(\epsilon_b)$  are the spontaneous/piezoelectric polarization, the length, and the static dielectric constant of well (barrier), respectively.

There are several techniques used to solve the effective mass equations for instance the finite difference method (FDM) [21], the propagation matrix method [18], and the basis expansion method [22]. FDM is used here because of its simplicity and easy implementation, especially for non-complex geometries.

In the process of implementation, differentiation operators are discretized to transfer the original problem to finite sets of linear equations. The first-order derivative  $d\psi/dz$  at a point  $z = z_i$  can be approximated as

$$\left(\frac{\partial\psi}{\partial z}\right)_i = \frac{\psi_{i+1} - \psi_{i-1}}{2\Delta z} \quad (10)$$

where  $\Delta z$  is the difference between adjacent grid points  $i$  and  $i + 1$  corresponding to mesh point  $z_i$  and  $z_{i+1}$ . Using a three-point central difference representation for the second-order derivatives, the central difference is

$$\left(\frac{\partial^2\psi}{\partial z^2}\right)_i = \frac{\psi_{i+1} - 2\psi_i + \psi_{i-1}}{\Delta z^2} \quad (11)$$

The resulted linear equations are solved using different numerical techniques such as the direct method (LU) decomposition or the iterative Newton method in the case of the Poisson equation and the Eigen decomposition of a matrix for the Schrödinger equation.

### 3. Software description

Aestimo 1D is programmed in Python Version 3.x [23] and because this is an interpreted computer language, there is no need for compiling. The source code is open-source, therefore the user can change it, improve it, and even redistribute it. Aestimo uses some well-known Python libraries like *scipy* [24], *numpy* [25], *cython* [26], and *matplotlib* [27] to perform accurate and faster calculations and present graphs to users.

The working scheme of the software is shown in Fig. 2. Before running the software, the user must edit *config.py* for some general numerical settings and to point the input file. The input file includes the structure and related settings of the structure. In addition to *config.py* and the related input file, the *database.py* file is also important for the calculation. All material parameters for semiconductor materials Si, Ge, GaAs, AlAs, InAs, InP, GaP, AlP, GaN, InN, AlN, CdO, MgO, ZnO, AlGaAs, InGaAs, InAsP, GaAsP, InGaP, AlInP, AlGaIn, InGaIn, AlInN, MgZnO, CdZnO, InGaAsP, AlGaInN are provided with the distribution [18,28–32].

There are several runnable scripts in the distribution (i.e. *aestimo.py* for conduction band only calculations, *aestimo\_eh.py* for conduction, and valence band calculations.). Once executed, the software firstly looks at *config.py* for the settings. The settings, the input file, and all necessary material parameters from *database.py* are loaded. Then, the software loads the necessary Python modules for calculation and performs the calculation. After calculation, all results and logs (with possible warnings and errors) are saved in the output folder, and the results are also drawn on the screen.

### 4. Applications

To test the validity of Aestimo 1D's physical model and computation scheme, comparison simulations with other software have been performed (see Appendix for Layer Materials and Parameters used in these examples). The examples presented are intended to demonstrate the accuracy of the multiband k.p model. The second and third examples also test the implementation of strain and spontaneous-piezoelectric built-in field effects.

The first example is shown in Fig. 3, it compares the results of a GaAs quantum well calculated with the *nextnano*<sup>3</sup> software [33]. Similar inputs were given to Aestimo's multiband model including ion implantation using Lindhard, Scharff, and Schjøtt (LSS) theory [34], but a calibration adjustment to the fixed doping values needed to be made to account for the incomplete ionization model implemented in *nextnano*<sup>3</sup>.

The produced results are in fair agreement with *nextnano*<sup>3</sup> results;

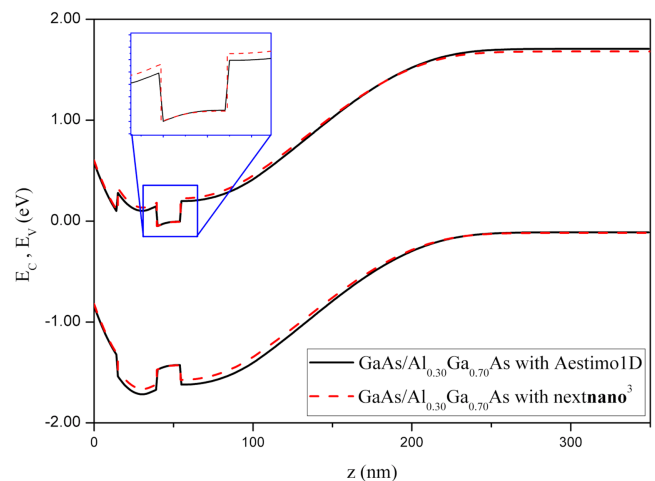


Fig. 3. Conduction and valence band edges for a GaAs QW. The x-axis shows the depth from the surface of the investigated structure.

Table 2

Comparison of electron state energies in the example GaAs QW's conduction band.

Electron states	Aestimo 1D	nextnano <sup>3</sup> [33]	Greg Snider's code [35]
E <sub>1</sub> (meV)	-0.1	-3.0	-1.3
E <sub>2</sub> (meV)	43.6	43.5	44.0
E <sub>3</sub> (meV)	117.1	117.5	117.8

Fig. 3 presents the self-consistent solution of Schrödinger-Poisson equations for the two simulators. The electron state energies presented in Table 2 for Aestimo 1D, *nextnano*<sup>3</sup>, and also the program written by Greg Snider [35] shows that there are some differences due to strain energy shifts between the programs' outputs but that there are consistent inter-subband energy gaps.

A second example shown in Fig. 4 is a simulation about the influence of surface states on the two-dimensional electron gas in an AlGaIn/GaN heterojunction field-effect transistors published by B. Jogai [36]. Aestimo 1D's multiband calculations are in agreement with *nextnano*<sup>3</sup> simulation [33] and Jogai's work [36]. This simulation confirms the accuracy of the strain and the spontaneous-piezoelectric built-in field models used in Aestimo 1D.

In Fig. 5, a double QW InGaIn/GaN structure has been simulated using Aestimo 1D's multiband model versus software called 1D-DDCC [37], this example demonstrates the ability of Aestimo 1D to work with

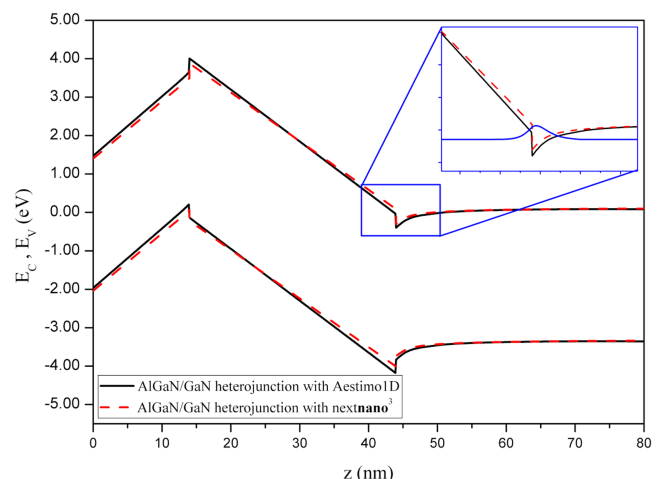


Fig. 4. Conduction and valence band edges for an AlGaIn/GaN heterojunction.

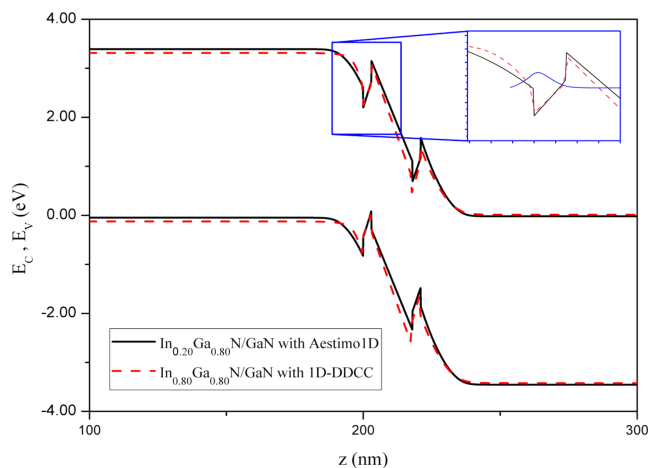


Fig. 5. Conduction and valence band edges for a double QW InGaN/GaN.

multi-quantum well (MWQ) structures taking in consideration strain-induced pyroelectric and piezoelectric built-in fields. The results are quite similar to matching inputs except for a minor adjustment to the fixed doping values as in the previous case.

Being an open-source code gives users the ability to introduce any form of customization through new theoretical models and numerical schemes, which is rare in commercial software and limited in cases. As a calculator, Aestimo 1D uses some methods and settings which can result in a difference concerning other calculators. In multi-quantum calculation, Aestimo 1D automatically takes the anti-crossing distance into consideration with a user-defined setting. Aestimo 1D uses the extrapolated-convergence-factor method (Stern damping) instead of the fixed-convergence-factor method, which reduces the convergence steps significantly. It also can calculate each quantum well's variables

## Appendix

Table A.1. Layer materials and parameters of Example 1.

Layer Structure	Layer thickness (nm)	Doping density ( $\text{cm}^{-3}$ )
p-Al <sub>0.3</sub> Ga <sub>0.7</sub> As	250	$0.8 \times 10^{17}$
Al <sub>0.3</sub> Ga <sub>0.7</sub> As	50	0.0 (LSS doping)
GaAs	15	0.0 (LSS doping)
Al <sub>0.3</sub> Ga <sub>0.7</sub> As	5	0.0 (LSS doping)
Al <sub>0.3</sub> Ga <sub>0.7</sub> As	20	0.0 (LSS doping)
n-GaAs	15	$0.8 \times 10^{17}$

Table A.2. Layer materials and parameters of Example 2.

Layer Structure	Layer thickness (nm)	Doping density ( $\text{cm}^{-3}$ )
i-GaN	14	0.0
i-Al <sub>0.3</sub> Ga <sub>0.7</sub> N	30	0.0
i-GaN	40	0.0

Table A.3. Layer materials and parameters of Example 3.

Layer Structure	Layer thickness (nm)	Doping density ( $\text{cm}^{-3}$ )
p-GaN	200	$1.8 \times 10^{19}$
n-In <sub>0.2</sub> Ga <sub>0.8</sub> N	3	$0.2 \times 10^{17}$
n-GaN	15	$0.2 \times 10^{17}$
n-In <sub>0.2</sub> Ga <sub>0.8</sub> N	3	$0.2 \times 10^{17}$
n-GaN	300	$2.0 \times 10^{18}$

separately or combined.

## 5. Conclusion

In this study, we report on an open-source general-purpose self-consistent 1D Schrödinger-Poisson equation solver, which can be used to study the electronic and some optical properties of semiconductor heterostructures, called Aestimo 1D. We briefly mentioned some of the main equations implemented in the Aestimo 1D and compare simulations with other known simulators to demonstrate the validity of the implemented models in the software.

## CRediT authorship contribution statement

**H. Hebal:** Software, Methodology, Writing - original draft, Writing - review & editing. **Z. Koziol:** Visualization, Writing - original draft. **S.B. Lisesivdin:** Conceptualization, Supervision, Writing - original draft, Writing - review & editing. **R. Steed:** Software, Methodology, Writing - original draft.

## Declaration of Competing Interest

The authors declare that they have no known competing financial interests or personal relationships that could have appeared to influence the work reported in this paper.

## Acknowledgments

Author names are listed in alphabetical order. SBL was supported in part by the Distinguished Young Scientist Award of the Turkish Academy of Sciences (TUBA-GEBIP 2016). SBL gratefully acknowledges the support of B. Sarikavak-Lisesivdin.

## Data availability

The raw data required to reproduce these findings are included in the software which can be downloaded from [<https://github.com/aestimosolver/aestimo/releases/download/v2.0/aestimo-v.2.0-master.zip>].

## Appendix A. Supplementary data

Supplementary data to this article can be found online at <https://doi.org/10.1016/j.commatsci.2020.110015>.

## References

- [1] S. Nicoletti J.M. Fédéli M. Fournier P. Labeye P. Barrिताult A. Marchant A. Glière A. Teulle J.G. Coutard L. Duraffourg June. Challenges in the miniaturization of Mid-IR sensors fully integrated on Si 2019 Optical Society of America (p. jsvi\_2,3).
- [2] H.S. Wasisto, J.D. Prades, J. Gülink, A. Waag, Beyond solid-state lighting: Miniaturization, hybrid integration, and applications of GaN nano-and micro-LEDs, *Appl. Phys. Rev.* 6 (4) (2019) 041315.
- [3] Sahm, A., Baumgärtner, S., Hofmann, J., Leisching, P. and Paschke, K., 2018, February. Miniaturized semiconductor MOPA laser source at 772 nm for the generation of UV laser light. In *Integrated Optics: Devices, Materials, and Technologies XXII* (Vol. 10535, p. 1053521). International Society for Optics and Photonics.
- [4] H.H. Radamson, X. He, Q. Zhang, J. Liu, H. Cui, J. Xiang, Z. Kong, W. Xiong, J. Li, J. Gao, H. Yang, Miniaturization of CMOS, *Micromachines* 10 (5) (2019) 293.
- [5] T.J. Walls, V.A. Sverdlov, K.K. Likharev, MOSFETs below 10nm: quantum theory, *Physica E* 19 (1–2) (2003) 23–27.
- [6] J.S. Yoon, J. Jeong, S. Lee, R.H. Baek, Sensitivity of Source/Drain Critical Dimension Variations for Sub-5-nm Node Fin and Nanosheet FETs, *IEEE Trans. Electron Devices* 67 (1) (2019) 258–262.
- [7] B. Sarikavak-Lisesivdin, Numerical optimization of two-dimensional electron gas in  $Mg_xZn_{1-x}O/ZnO$  heterostructures ( $0.10 < x < 0.30$ ), *Phil. Mag.* 93 (9) (2013) 1124–1131.
- [8] G. Atmaca, P. Narin, B. Sarikavak-Lisesivdin, S.B. Lisesivdin, Two dimensional electron gas in a hybrid GaN/InGaN/ZnO heterostructure with ultrathin InGaN channel layer, *Physica E* 79 (2016) 67–71.
- [9] P. Harrison, A. Valavanis, Quantum wells, wires and dots: theoretical and computational physics of semiconductor nanostructures, John Wiley & Sons, 2016.
- [10] H. Hebal, H. Abid, Crystal orientation effects on electronic and optical properties of wurtzite ZnO/CdZnO quantum well lasers, *Superlattices Microstruct.* 75 (2014) 866–878.
- [11] Erucar, T., Nutku, F., Donmez, O. and Erol, A., 2017, February. Electronic band-structure of semiconductor dilute bismide structures. In *AIP Conference Proceedings* (Vol. 1815, No. 1, p. 050004). AIP Publishing LLC.
- [12] C. Cetinkaya, E. Cokduygular, F. Nutku, O. Donmez, J. Puustinen, J. Hilska, A. Erol, M. Guina, Optical properties of n-and p-type modulation doped GaAsBi/AlGaAs quantum well structures, *J. Alloy. Compd.* 739 (2018) 987–996.
- [13] M.M. Bajo, J. Tamayo-Arriola, M. Hugues, J.M. Ulloa, N. Le Biavan, R. Peretti, F.H. Julien, J. Faist, J.M. Chauveau, A. Hierro, Multisubband plasmons in doped Zn O quantum wells, *Phys. Rev. Appl.* 10 (2) (2018) 024005.
- [14] B. Meng, J. Tamayo-Arriola, N. Le Biavan, M.M. Bajo, A. Torres-Pardo, M. Hugues, D. Lefebvre, A. Hierro, J.M. Chauveau, J. Faist, Observation of Intersubband Absorption in Zn O Coupled Quantum Wells, *Phys. Rev. Appl.* 12 (5) (2019) 054007.
- [15] M.M. Bajo, J. Tamayo-Arriola, N. Le Biavan, J.M. Ulloa, P. Vennéguès, D. Lefebvre, M. Hugues, J.M. Chauveau, A. Hierro, Breaking the Intersubband Selection Rules for Absorption with Zn O Quantum Wells: Light Polarization Sensitivity under Normal Incidence, *Phys. Rev. Appl.* 10 (3) (2018) 034022.
- [16] D.F. Nelson, R.C. Miller, D.A. Kleinman, Band nonparabolicity effects in semiconductor quantum wells, *Physical Review B* 35 (14) (1987) 7770.
- [17] T. Ando, H. Taniyama, N. Ohtani, M. Nakayama, M. Hosoda, Self-consistent calculation of subband occupation and electron–hole plasma effects: Variational approach to quantum well states with Hartree and exchange–correlation interactions, *J. Appl. Phys.* 94 (7) (2003) 4489–4501.
- [18] S.L. Chuang, S.L. Chuang, *Physics of optoelectronic devices*, Wiley, 1995, p. 183.
- [19] A. Bykhovski, B. Gelmont, M. Shur, Strain and charge distribution in GaN-AlN-GaN semiconductor-insulator-semiconductor structure for arbitrary growth orientation, *Appl. Phys. Lett.* 63 (16) (1993) 2243–2245.
- [20] S.H. Park, S.L. Chuang, Comparison of zinc-blende and wurtzite GaN semiconductors with spontaneous polarization and piezoelectric field effects, *J. Appl. Phys.* 87 (1) (2000) 353–364.
- [21] D. Ahn, S.H. Park, *Engineering quantum mechanics*, John Wiley & Sons, 2011.
- [22] G.E. Bauer, T. Ando, Exciton mixing in quantum wells, *Physical Review B* 38 (9) (1988) 6015.
- [23] T.E. Oliphant, Python for scientific computing, *Comput. Sci. Eng.* 9 (3) (2007) 10–20.
- [24] Virtanen, P., Gommers, R., Oliphant, T.E., Haberland, M., Reddy, T., Cournapeau, D., Burovski, E., Peterson, P., Weckesser, W., Bright, J. and van der Walt, S.J., 2020. SciPy 1.0: fundamental algorithms for scientific computing in Python. *Nature Methods*, 17(3), pp.261-272.
- [25] S.V.D. Walt, S.C. Colbert, G. Varoquaux, The NumPy array: a structure for efficient numerical computation, *Comput. Sci. Eng.* 13 (2) (2011) 22–30.
- [26] S. Behnel, R. Bradshaw, C. Citro, L. Dalcin, D.S. Seljebotn, K. Smith, Cython: The best of both worlds, *Comput. Sci. Eng.* 13 (2) (2011) 31–39.
- [27] J.D. Hunter, Matplotlib: A 2D graphics environment, *Comput. Sci. Eng.* 9 (3) (2007) 90–95.
- [28] S. Adachi, *Properties of semiconductor alloys: group-IV, III-V and II-VI semiconductors*, 2009.
- [29] C. Hamaguchi, *Basic semiconductor physics*, Springer-Verlag, Berlin, 2010.
- [30] T.D. Steiner, *Semiconductor nanostructures for optoelectronic applications*, Artech House, 2004.
- [31] I. Vurgaftman, J.R. Meyer, Band parameters for III–V compound semiconductors and their alloys, *J. Appl. Phys.* 89 (11) (2001) 5815–5875.
- [32] I. Vurgaftman, J.N. Meyer, Band parameters for nitrogen-containing semiconductors, *J. Appl. Phys.* 94 (6) (2003) 3675–3696.
- [33] S. Birner, S. Hackenbuchner, M. Sabathil, G. Zandler, J.A. Majewski, T. Andlauer, T. Zibold, R. Morschl, A. Trellakis, P. Vogl, Modeling of Semiconductor Nanostructures with nextnano3, *Acta Physica Polonica Series A* 110 (2) (2006) 111.
- [34] J. Lindhard, M. Scharff, H.E. Schiött, Range concepts and heavy ion ranges, Munksgaard, Copenhagen, 1963, pp. 1–42.
- [35] I.H. Tan, G.L. Snider, L.D. Chang, E.L. Hu, A self-consistent solution of Schrödinger-Poisson equations using a nonuniform mesh, *J. Appl. Phys.* 68 (8) (1990) 4071–4076.
- [36] B. Jogai, Influence of surface states on the two-dimensional electron gas in AlGaIn/GaN heterojunction field-effect transistors, *J. Appl. Phys.* 93 (3) (2003) 1631–1635.
- [37] Wu, Y.-R., 2015. One Dimensional Poisson, Drift-Diffusion, and Schrödinger Solver (1D-DDCC), Technical Report, National Taiwan University. (unpublished) (code can be found at <http://yrwu-wk.ee.ntu.edu.tw/index.php/ddcc-1d/>).